Precision Prediction of Microbial Ecosystem Impact on Host Metabolism Using Genome-Resolved Metagenomics

Mohamed Mohssen†[1,2,3,4], Ahmed A. Zayed†[2,3,4], Kristina A. Kigerl†[5,6], Jingjie Du[2,¥], Garrett J. Smith[2,3], Jan M. Schwab[5,6], Matthew B. Sullivan*[1,2,3,4,7] and Phillip G. Popovich*[3,5,6]

1 The Interdisciplinary Biophysics Graduate Program, The Ohio State University, Columbus, Ohio 43210, USA

2 Department of Microbiology, The Ohio State University, Columbus, Ohio 43210, USA

3 Center of Microbiome Science, The Ohio State University, Columbus, Ohio 43210, USA

4 EMERGE Biology Integration Institute, The Ohio State University, Columbus, Ohio 43210, USA

5 Department of Neuroscience, The Ohio State University Wexner Medical Center, Columbus, OH, 43210, USA

6 Belford Center for Spinal Cord Injury, The Ohio State University Wexner Medical Center, Columbus, OH, 43210, USA

7 Department of Civil, Environmental and Geodetic Engineering, The Ohio State University, Columbus, OH 43210, USA

¥ Current Address: Division of Nutritional Sciences, Cornell University, Ithaca, NY, 14850, USA

† These authors contributed equally

* Correspondence: phillip.popovich@osumc.edu and sullivan.948@osu.edu

Abstract

Microorganisms often drive ecosystem function, yet precision disturbance response and ecosystem impact predictions remain challenging due to poorly captured ecological and metabolic interconnectedness and functional redundancy. For example, while mammalian gut dysbiosis is recognized to influence host metabolism, key microbiota and mechanisms governing their effects remain poorly understood. Here we developed a genome-resolved eco-systems biology workflow to predict how gut microbial metabolism affects mammalian health, and we applied it to a 'spinal cord-gut axis' dataset. By scaling and integrating temporally resolved network analytics and consensus statistical approaches, we identified largely previously uncharacterized microbial species that best predict host physiology following neurological impairment. *In silico* validation through "complete" pathway-centric and comparative genomic analyses revealed that among these species, the major encoded microbial metabolic changes were in pathways directly linked to host nitrogen balance, and they varied by host sex and microbial ecotype/species. Moreover, we identified the exact bacterial species (and their draft genome sequences) driving urease-dependent versus amino acid-dependent nitrogen gut metabolism – findings that explain previously mechanistically-ambiguous, but clinically relevant, ammonia-driven host nitrogen imbalance. More broadly, these ecology- and community-aware approaches provide a framework to study dynamic, interconnected microbiomes that advances from enrichment-based single-taxon and single-gene correlations towards building microbe(s)-driven mechanistic insights that integrate community context and whole pathways.

Main text

Introduction

Earth systems are inhabited by microorganisms that perform key elemental transformations, including those related to carbon[1,2] and nitrogen[3] cycling. In these systems, ecological context is critical for understanding microbiota functioning, especially when it comes to microbial adaptations to particular niches[4]. While gene marker approaches provide incredibly valuable microbial community composition data for new ecosystems studied, genome-resolved approaches are emerging as the gold standard where it is critical to capture the fast-evolving, niche-defining functions that dictate ecosystem functioning and that marker genes miss[5–14], particularly essential for translating the microbiome in health and disease[13,15–17]. Additionally, microbiomes are dynamic and highly interconnected as microbes exchange and compete for metabolites and other molecules in their environment[18,19] (e.g., the gut[20]).

Despite the growing appreciation of microbial contributions to gut ecosystem function, current approaches to study these systems largely focus on microbiota constituents in isolation (i.e., linking a single taxon/gene at a time to health/disease), often ignoring complex and dynamic whole community interactions. Recently, specific microbes have been identified to significantly impact health and disease, including *Faecalibacterium* species in inflammatory bowel diseases and colorectal cancer (reviewed in[21]), *Hominenteromicrobium* strain YB328 in enhancing anti-tumour immunity[22], and several others (reviewed in[6,23]). However, such microbes undoubtedly rely on ecosystem-dependent metabolic interactions within the microbial community, with a recently elucidated example being carbon-based metabolic interplay for beneficial *Lactobacillus johnsonii*[24]. Beyond genomic representation at the community level, gut bacterial gene expression profiles are also emerging as taxon-context-dependent[25]. Thus, even if one taxon leads to significant health benefits under an experimental condition(s), ignoring microbe-microbe interactions limits the generalizability and modulation of microbe-mediated interventions. This calls for an eco-systems biology approach[26] whereby data generation captures genome-wide variation (including ecosystem-specific, niche-defining traits) and scalable, hypothesis-free

analytics account for complex functional redundancies and microbial interactions community-wide to best estimate ecosystem functioning.

Here we sought to establish such a "data-driven" workflow to (i) better identify emergent ecosystem properties that elucidate precise microbial contributions to host health and disease and (ii) apply this workflow to a biomedically-relevant dataset as a case study. To do this, we focused on neurological impairment (NI) as a gut ecosystem "environmental" challenge[27–34] that alters mammalian host metabolism[35,36]. This systematic workflow developed to investigate microbe-host interactions requires no *a priori* assumptions and uses (i) cross-validated eco-systems biology analytics, including machine learning, to identify key ecosystem-impacting microbial taxa, and (ii) consensus genome-resolved, pathway-centric (i.e., requiring multiple genes involved in a pathway/function) analyses to elucidate metabolism-based mechanisms underpinning these ecosystem impacts. These requirements to evaluate enriched functions in community and pathway context take a critical step from pairwise correlations towards systems-level functional assessments of causation and mechanism. Case study application of this data-driven approach highlights key microbial species and metabolic "complete" pathways influencing mammalian host nitrogen metabolism and provides insights into potential therapeutic targets for future *in vivo* validation.

Emergent gut microbial networks predict host physiology

We previously established a well-controlled spinal cord-gut axis murine model system[24] that represents NI and includes high-resolution gut metagenome temporal sampling, and we manually reconstructed carbon-based microbial metabolic connectivity in the gut ecosystem to inform microbe-microbe interactions. To evaluate microbe-host metabolic interactions in a whole-ecosystem context, we leverage the curated Mouse B6 Gut Catalog (MB6GC)[24], which includes 263 dereplicated metagenome-assembled genomes (MAGs) recovered from fecal and cecal samples temporally obtained from male and female mice with graded levels of NI caused by spinal lesions at mid- (T10) or high- (T4) thoracic spinal levels. Such lesions partially or completely disrupt neural control over the gut. Mice receiving spinal surgery, but without a spinal cord lesion, served as a control group ("Lam") (see[24] for full study design). These MAGs, which represented the *in-situ* gut microbial community quite well (i.e., they recruited ~80% of the total metagenomic

reads), were quantified over 6 months across groups and evaluated against a standardized scale of neurological function in mice (Basso Mouse Scale, or BMS, for locomotion) as a proxy for overall mouse physiological state.

To analyze these data considering the full microbial community context, we applied an eco-systems biology approach (*sensu*[37]) that uses MAG-based relative abundance data to organize the microbial community into predictably interacting (e.g., competing or cross-feeding) sub-communities of co-occurring MAGs via weighted gene/genome correlation network analysis (WGCNA)[38]. Longitudinal sample-dependencies were accounted for by generating six independent networks – one for each timepoint across 6 months following NI (see **Fig. 1A**, **Fig. S1**, and "*WGCNA Analysis"* in the **Methods** for more details). The resulting initial networks were power-transformed to identify robust subnetworks (i.e., modules) meant to represent microbial sub-communities whose members co-vary and therefore possibly interact. Each subnetwork was then correlated with host neurological function (BMS scores) such that member taxa of correlating subnetworks could be analyzed via leave-one-out cross-validation to identify members critical for these associations. Specifically, leave-one-out cross-validation via partial least square (PLS) regression analysis assigned variable importance in projection (VIP) scores to each taxon to identify key MAG(s) (i.e., critical for these correlations) within each emergent subcommunity (see **Fig. 1A** inset), in effect linking member taxa with host health. We generalized this cross-validated PLS-VIP approach to all emergent sub-communities, using the consensus of multiple statistical techniques, cross-validation methods, and manual inspection (see "*WGCNA analysis*" in **Methods**) to identify key MAGs inferred to drive ecosystem changes, hereafter named "PLS-VIP MAGs". Only MAGs from male mice networks met the strict criteria of the PLS-VIP MAGs (sex-specific taxon and functional changes are detailed elsewhere[24]).

Application of this workflow to MB6GC MAGs derived from mice with or without NI revealed the following. For non-perturbed gut ecosystems in healthy mice with intact spinal cords, there were no emergent sub-communities at Day 0, confirming similar baseline microbial communities. However, subsequent time points revealed multiple emerging sub-communities after NI (**Fig. 1A**). In total, 19 consensus PLS-VIP MAGs were identified that likely control ecosystem dynamics and function after disrupting spinal cord-gut crosstalk (**Fig. 1**). Of these 19 PLS-VIP MAGs (**Fig. 1B-C**), 11 MAGs from the Firmicutes_A phylum increased in abundance (Group 1

129 MAGs), whereas 8 MAGs from 4 separate phyla decreased (Group 2 MAGs). Six of the 19 MAGs
130 had strong associations with health or disease states based on prior studies, and of these six MAGs,
131 five decreased in our data (*Lactobacillus Johnsonii*, Turicibacter sp002311155, *Parasutterella*
132 *excrementihominis*, CAG-485 sp002362485, and CAG-873 sp910577315) and one increased
133 (Acetatifactor sp003612485) after lesioning the spinal cord. Specifically, for these 6 "known"
134 MAGs, published data indicate that these microbes can significantly affect host physiology: (i) *L.*
135 *johnsonii* enhances gut barrier integrity[39] and gut mucosal immunity[40], and reduces plasma total
136 cholesterol levels[41]; (ii) Turicibacter sp002311155 was reduced after murine lung cancer in mice[42]
137 and strains of the Turicibacter genus differentially modify bile acids and lipid metabolism[43]; (iii)
138 *P. excrementihominis,* a core component of human and murine microbiomes with roles in bile acid
139 maintenance and in cholesterol and tryptophan metabolism, is reduced by high-fat-diet[44]; (iv)
140 CAG-485 sp002362485 (recently proposed as "*Sangeribacter muris*" and biochemically
141 characterized in[45]) is one of the most dominant and prevalent species in the murine gut and may
142 protect from intestinal colitis[45]; (v) similar to *P. excrementihominis*, CAG-873 sp910577315
143 decreased after high-fat-diet in mice[46], whereas (vi) Acetatifactor sp003612485 levels were
144 positively correlated with plasma metabolites implicated in cardiovascular diseases[47]. However,
145 while 6 of the PLS-VIP-identified MAGs have previous ties to health and disease in other model
146 systems, our data-driven analyses not only recovered these, but also identified 13 additional MAGs
147 that could have relevance to mammalian host health. Notably, these 19 species-level MAGs were
148 critical to "predict" NI (BMS scores) – due not only to individual abundance changes (perhaps
149 captured by standard pairwise enrichment assessments), but also adding in two more layers of
150 conservative assessment that take into account microbe-microbe co-variation and leave-one-out
151 cross-validation.

152 Inferring microbial community metabolic output driven
153 by key network-emergent taxa

154 Since microbiomes are functionally redundant (i.e., sharing metabolic blueprints) and
155 metabolically connected (i.e, cross-feeding[48]), we assessed how PLS-VIP MAGs might impact
156 host (patho)physiology by analyzing PLS-VIP MAGs' functional potential in the context of the
157 entire gut microbial community (PLS-VIP MAGs + other community members) metabolism.

158 Instead of relying on changes in single genes, we considered our basic unit to be that of a function,
159 pragmatically represented as genes mapping to metabolic pathways (i.e., expert defined, conserved
160 functional unit of multiple genes). Specifically, we estimated relative abundances of microbial
161 metabolic functions (see **Fig. 2A** and **Methods**) and identified metabolic pathways fulfilling two
162 criteria: (i) those with relative abundances that significantly changed in mice with NI (vs. sham
163 controls) even against community-wide changes (i.e., summing abundances of *all* recovered
164 MAGs encoding these pathways) (**Fig. S2-3**), and (ii) those that were differentially encoded
165 between PLS-VIP MAG groups that increased or decreased in mice with NI as determined by a
166 statistical enrichment analysis (see **Fig. S4** and **Methods**). To identify PLS-VIP MAG-dependent
167 pathway-level changes and minimize pathways functionally compensated by other community
168 members, only pathways meeting both criteria were analyzed further.

169 Identifying PLS-VIP MAG-dependent pathways proceeded as follows. *First*, Anvi'o[49] was
170 used to functionally annotate (see "*Anvi'o pathway identification"* in **Methods**) all 263 MAGs
171 against the KEGG database and organize these annotations (KEGG Ortholog [KO] numbers) into
172 hierarchical KEGG modules that represent partial or complete metabolic pathways. *Second*,
173 module completeness (*sensu*[50], see **Methods**) was estimated per MAG from the constituent KEGG
174 genes present in it (**Fig. S4A**). *Third*, using abundances of complete modules, a time-resolved,
175 whole-community differential analysis was performed (see "*Fold-change calculation for*
176 *visualizing pathways"* in **Methods**). This analysis revealed that 26 modules (**Fig. 2B**), as defined
177 by hierarchical clustering (**Fig. S2A**; see all modules in **Fig. S2-3**), encompassed the largest
178 observed module changes in mice with NI, regardless of spinal lesion level or sex. Thus, these 26
179 modules represent *whole-community* metabolic changes. *Finally,* and independently, a generalized
180 linear model[51] within Anvi'o (see "*Pathway enrichment analysis with Anvi'o*" in **Methods**) was
181 used to quantify the enrichment of each KEGG module across Group 1 (increasing following NI)
182 and 2 (decreasing) PLS-VIP MAGs. This enrichment analysis identified 52 modules as
183 differentially encoded by the two PLS-VIP MAG groups (**Fig. S4B**).

184 The intersection of these 52 PLS-VIP MAG-level and 26 whole community-level findings
185 identified 19 complete VIP-driven modules (**Fig. 2B**) that represent the largest abundance-based
186 microbial metabolic changes in mice with NI driven by PLS-VIP MAGs and effectively "ranked"
187 by impact and change direction. We hereafter refer to these modules as "Community VIP (cVIP)-

188 driven modules". Of these, six modules (**Fig. 2B**) belong to interconnected themes of microbial
189 metabolism critical for host nitrogen metabolism, namely ammonia/urea and amino
190 acid/polyamine metabolisms. Because mammalian physiology related to health/disease is typically
191 correlated with nitrogen balance[36], where net nitrogen gain and loss are associated with health and
192 disease, respectively, we sought to explore these six modules as most system-relevant.

193 Gut microbial nitrogen metabolism disruption by 194 neurological impairment

195 Among the 19 cVIP-driven modules, one module involved in bacterial fixation of inorganic
196 nitrogen (dissimilatory nitrate reduction, via nitrite, to *ammonia*, hereafter DNRA; KEGG module
197 M00530) was significantly reduced in mice with NI (**Fig. 2B**) and was solely encoded by *P.*
198 *excrementihominis* among the PLS-VIP MAGs (**Fig. S4**). DNRA enables the retention of scarce
199 nitrogen as soluble ammonia in organic-rich and anoxic ecosystems[52] and is considered a major
200 pathway for nitrate reduction by bacteria in rumen and human intestine[53–56].

201 In mice with NI, we also observed a significant reduction in the bacterial organic nitrogen
202 pathway for urea nitrogen salvaging (UNS) involved in degrading *urea* to ammonia via urease
203 genes. UNS by gut microbes likely has an appreciable role in mammalian nitrogen metabolism[57,58],
204 albeit typically treated as a "black box". Indeed, mammals cannot acquire or "fix" nitrogen from
205 the atmosphere like microbes, so they obtain it mostly from dietary proteins, which they then
206 catabolize into nitrogen-rich compounds like amino acids and ammonia. Although the liver is the
207 primary site where protein is metabolized and ammonia detoxified, intestinal bacteria might also
208 participate in nitrogen metabolism as previously suggested and as evidenced from our data as
209 described below.

210 In our system, we inspected urease-encoding bacteria by manually reconstructing the
211 urease pathway up from single-gene annotations (*sensu*[59]; it is absent from the KEGG hierarchy),
212 and then genome-contextualizing the pathway (as above for cVIP-driven modules). This revealed
213 that, among PLS-VIP MAGs, 100% of the urease pathway was encoded by only CAG-485
214 sp002362485 and CAG-873 sp910577315. These two MAGs were highly dominant as their

median relative abundances represented >35% or ~16-20% of the microbial community in healthy (i.e., Lam) or male mice with NI, respectively (**Fig. 3A-B**). Further, only four other MAGs, collectively accounting for <1% of the entire microbial community, encoded this complete pathway (**Fig. 3B**). Notably, other MAGs from the same family of the two urease-encoding PLS-VIP MAGs (Muribaculaceae) lacked urease genes (**Fig. 3A**). This suggests relatively recent functional trait evolution in CAG-485 sp002362485 and CAG-873 sp910577315 ecotypes, which would be missed using marker-gene predictions[60]. The relative abundance of these two MAGs was less prominent in healthy female mice (baseline <20% median relative abundance) and less affected by NI. Instead, other non-urease-encoding Muribaculaceae (i.e., Duncaneilla MAGs) dominated the gut of healthy female mice and were significantly decreased in female mice with NI (**Fig. 3B**). These data suggest sex-specific species-driven microbiota-host metabolic interactions, which impacts generalizability of single-sex experiments seeking to assess microbiome impacts.

Finally, our data revealed significant spinal cord-dependent changes in cVIP-driven modules encoding *amino acids* and *polyamines*. cVIP-driven modules encoding the amino acids tyrosine and phenylalanine, rather than tryptophan[34], were significantly reduced (**Fig. 2B**, **Fig. 4**). Among PLS-VIP MAGs, only *P. excrementihominis* encoded 100% of these pathways (**Fig. S4**). Conversely, other cVIP-driven modules increased significantly in NI mice. Those modules encode *polyamine* precursors – the amino acids arginine and ornithine – as well as polyamines themselves (**Fig. 2B**, **Fig. 4**). Taxonomically, these biosynthesis pathways were well-represented in Group 1 PLS-VIP MAGs (increasing after NI; 2/11 for polyamine, 11/11 for arginine, and 10/11 for ornithine) but were sparse in Group 2 PLS-VIP MAGs (decreasing after NI; 0/8 for polyamine, and 2/8 for arginine and ornithine) (**Fig. S4**).

Discussion

This work provides a scalable genome-resolved, functionally contextualized eco-systems biology analytical framework that takes another step away from simple (single-gene/genome/feature) correlations, which fail to consistently infer microbe-host interactions in complex system like the gut[61], and towards inferred causation and/or mechanism between community-contextualized microbes and host health. The first step in this workflow scales up and

244 semi-automates eco-systems biology approaches developed in another complex ecosystem (i.e.,
245 the oceans[37]) to organize taxa or metabolic functions to assess interacting subsets, evaluate their
246 predictive power of ecosystem properties (e.g. carbon flux in the oceans or disease status in
247 mammals), and cross-validate them to assess the specific taxa or functions that are most important
248 to these predictions. Notably, this workflow newly applies this eco-systems biology approach to
249 longitudinal datasets by controlling for temporal dependencies – a critical advance for time-
250 resolved microbiome studies. The second step in our workflow was to establish a mechanism for
251 robustness (i.e., consistency of each taxon's temporal abundance patterns) by curating identified
252 taxa (i.e., PLS-VIP MAGs) and removing those that were redundant across longitudinally
253 differentiated networks. Finally, the third advance in this workflow was to mechanistically and
254 functionally contextualize changes in consensus PLS-VIP MAGs. This was done by leveraging
255 genome-resolved "complete"-pathway functional signals from multiple data streams that together
256 considered consensus PLS-VIP MAG-based functional enrichment analysis in context of whole-
257 community-based functions. Together, these analyses reduce reliance on pairwise statistical
258 inferences to focus instead on identifying key taxa and complete pathways within community-
259 wide traits and modeled interactions.

260 Applied to a large-scale dataset from healthy or NI mice, our workflow revealed 19 key
261 whole-community-stabilizing gut bacterial members (i.e., PLS-VIP MAGs; **Fig. 1**) that are
262 influenced by NI and identified 19 microbial metabolic pathways that are modeled to drive
263 microbial ecosystem dynamics in NI mouse guts (**Fig. 2B**). We highlight six of these pathways
264 together with an *ad hoc* reconstructed UNS pathway – all centered around nitrogen metabolism –
265 that suggest and provide specific mechanistic hypotheses for how gut microbiota play a larger role
266 in influencing host nitrogen balance than previously recognized. We discuss here two specific
267 clinically relevant examples related to (i) ammonia biosynthesis and urea degradation pathways,
268 and (ii) altered amino acids and polyamines biosynthesis.

269 Towards the former nitrogen metabolism impact, NI significantly reduced the abundance
270 of specific dominant gut bacterial MAGs/species previously underappreciated for their role in
271 ammonia biosynthesis and urea degradation pathways (**Fig. 3**), presumably reducing microbially-
272 derived ammonia and elevating urea buildup in the host. The effect of urease-positive bacteria on
273 ammonia levels is supported by decades-long observations[62] and was recently mechanistically

validated and shown to have strong ties to host health[59], where reduction in bacterium-derived ammonia induced depressive-like behaviors and ammonia-mediated, glutamine-dependent dysfunctional neurotransmission in a (male) mouse depression/stress model[59]. Critically, the brain is the only implicated regulator in this literature. However, based on our data, system-wide changes (e.g., dysfunctional neurotransmission) are expected whenever there is spinal cord dysfunction (likely occurs in virtually all neurological diseases[27–33]) as maintaining organismal homeostasis requires sympathetic nervous system functioning that originates in the spinal cord. Since the spinal cord collects most peripheral tissue sensory information (either directly or later integrated), any nervous system perturbation will impair neurotransmission through the spinal cord and its subsequent control over systemic organs, including the gut. Thus, traumatic spinal cord injury (SCI), through changing microbiota, could alter host health. An example of such alterations is the NI-induced microbiota-mediated ammonia reduction and its subsequent urea accumulation as inferred from our data. Post-SCI uremia (urea buildup) is a common comorbidity in SCI patients that, so far, has been solely attributed to paralysis-dependent muscle catabolism and impaired renal function (based on male rat data[63]). Our data suggest that chronic reduction of gut urease-positive bacteria contribute to that comorbidity, which could also explain why even aggressive nutritional intervention[64,65] does not allow SCI patients to overcome negative nitrogen balance.

As discussed above, we show that the reduction in abundance of urease-positive bacteria was more pronounced in male mice compared to female mice as the two most abundant species in male mice (accounting for 35% of the baseline community) were urease-positive. Notably, literature reporting ammonia reduction[59] and urea accumulation[63] (similar to inferences from our data) used male mice/rats among studies predominately using female mice[5]. We posit that lower baseline levels of urease-positive bacteria in female mice (evidenced by the dominance of urease-negative members from the same family) indicate their lower dependency on the gut microbiome as an ammonia source, compared to males. Consistent with this are data showing that the rate of ammonia generation and recycling in the kidney are greater in female compared to male mice[66,67]. This highlights the importance of controlling for sex in microbiome studies and generates data-driven hypotheses for future experimental validation. Further, we uncover such results that explain cross-disciplinary observations using only a hypothesis-free computational approach, which pinpointed the exact genomes driving systems-level functional changes instead of relying on low-

304 resolution analyses (e.g., only up to family-level predictions of urease-positive bacteria[59] with little
305 ecological consistency; **Fig. 3**) or on well-characterized taxa that are either rare or transient (i.e.,
306 not part of the core microbiome)[59,68].

307 Towards the latter nitrogen metabolism impact, the abundance of gut bacterial MAGs
308 encoding aromatic and non-aromatic amino acids and polyamines also was significantly changed
309 in NI mice. First, biosynthesis of aromatic amino acids (tyrosine and phenylalanine) was inferred
310 to decrease following NI. These gut-bacteria-produced amino acids can enter circulation and
311 bypass blood-brain or blood-spinal cord barriers to be precursors for neurotransmitters (dopamine
312 and nor/epinephrine) critical for normal neurological function[69]. Second, biosynthetic pathways
313 for the non-aromatic, semi-essential amino acid arginine and for polyamines increased in NI mice.
314 Because arginine is used as a precursor for synthesizing polyamines and proteins[70], an increase in
315 gut microbial arginine biosynthesis, or its precursor ornithine, might benefit the host[71,72]. However,
316 literature from murine SCI models shows that an arginine boost may promote inflammation and
317 tissue injury (e.g., neurological recovery was impaired if mice received arginine supplements and
318 neurological function improved if arginine was depleted[73,74]). Similarly, although polyamines are
319 critical for cell growth and viability in mammals[72], they have been shown to be elevated in serum
320 of uremic patients[75]. Given this conflicting literature and our new findings, we posit that (i)
321 elevated polyamine levels contribute to urea accumulation as the polyamine biosynthetic process
322 releases urea and creates agmatine and/or putrescine (**Fig. 4**), and (ii) the two products (agmatine
323 and putrescine) could play both beneficial and harmful roles in the context of disease or injury to
324 the CNS[76,77].

325 Based on the data presented, we propose that increased blood urea associated with NI is
326 due to microbial shifts resulting from disrupted spinal cord-gut communication. Indeed, we see
327 shifts that include (i) a reduction of bacteria encoding urease (particularly in males) and
328 neurotransmitter precursors, and (ii) an increase in bacteria encoding health-critical amino acids
329 and polyamines. Shifting from pre-dysbiotic microbes synthesizing ammonia as their nitrogen
330 source to dysbiotic microbes synthesizing amino acids is consistent with previous reports showing
331 similar metabolic patterns in Clostridia-dominated gut microbiomes[62]. Consistent with this, our
332 data indicate that all 11 PLS-VIP MAGs that increase in NI mice guts belong to the class Clostridia,
333 as opposed to only 3 out of the 8 PLS-VIP MAGs decreasing in these same mice.

334 Finally, our work shows that understanding community context and interactions is essential
335 when making inferences about local and systemic effects of the gut microbiome (e.g., urea and
336 ammonia balance in the host). The specific example to demonstrate this is the PLS-VIP MAGs
337 identified here presumably serving as the main drivers of this microbial metabolism, with little to
338 no genetic evidence to suggest compensation by rare community members. The lack of community
339 compensation makes these PLS-VIP MAGs an ideal short-list of probiotic targets for future
340 experimental evaluation.

341 Conclusions

342 Medical microbiome research is calling for systems-level genome-resolved approaches
343 that help uncover mechanistic insights to translate the microbiome in health and disease[13,15–17].
344 This report demonstrates that spinal cord-mediated alterations in gut microbial metabolic potential
345 can significantly impact host nitrogen metabolism. These findings were uncovered using
346 our improved, hypothesis-free, data-driven workflow, which required no *a priori* assumptions or
347 knowledge. By leveraging scalable, genome-informed analytics, we identified a set of microbial
348 taxa, termed PLS-VIP MAGs, that best predict host physiological state and drive the community
349 nitrogen metabolism. While some PLS-VIP MAGs, like *L. johnsonii*, have known associations
350 with neurological outcomes, others are newly predicted to influence host metabolism despite
351 being rarely linked to neurological disorders or considered under the influence of spinal
352 sympathetic networks. If validated in relevant neurological disease models, perhaps a combination
353 of PLS-VIP MAGs could represent broadly impactful probiotics, given their demonstrated
354 metabolic functions (shown here) and ubiquity within the core gut microbiome[78,79]. Such
355 validation experiments represent the next grand challenge as, critically, they must recapitulate
356 community context, such as cross-feeding partners and competing niches, that is inherent in natural
357 microbiomes and captured in our now community-aware analytics. Success in this would empower
358 microbial therapeutics to restore nitrogen balance and alleviate characteristic CNS disease
359 symptoms where spinal cord-gut communication is impaired, including stroke, spinal injury,
360 multiple sclerosis, and myriad neurodegenerative diseases[64,65]. As a step towards this, experiments
361 guided by these approaches now show that restoring one PLS-VIP MAGs can prevent the onset of
362 metabolic and immune dysfunction caused by SCI[24].

More broadly, however, this report provides a roadmap for addressing a grand challenge in microbiome science whereby microbiota and their functions are more mechanistically linked with their environmental[1,80] and/or host[14,81,82] contexts. Given the challenges of *in-vivo*-representative synthetic communities experiments[83] (e.g., including all interacting partners), we query the natural community interactions across different 'environmental' conditions. We do this by shifting from global pairwise predictions about microbial functions based on conserved, slow-evolving marker genes (e.g., 16S rRNA genes) – which are likely evolutionarily out of sync with many ecological traits[5–14] – towards genome-, population-structure-[12] and community-informed functional predictions. In this way, our data-driven discovery process can better predict the fast-evolving, niche-defining traits that structure ecosystems and yet often vary significantly within genera and species[10,14]. Such analytical advances, alongside improved community metabolic modeling approaches to assess unintended consequences[84,85], will expedite the development of systems-level knowledge, which traditionally requires years to achieve but is critical to more fully realize the potential for microbiome engineering as a precise and context-specific therapeutic for personalized medicine.

MAIN FIGURES:

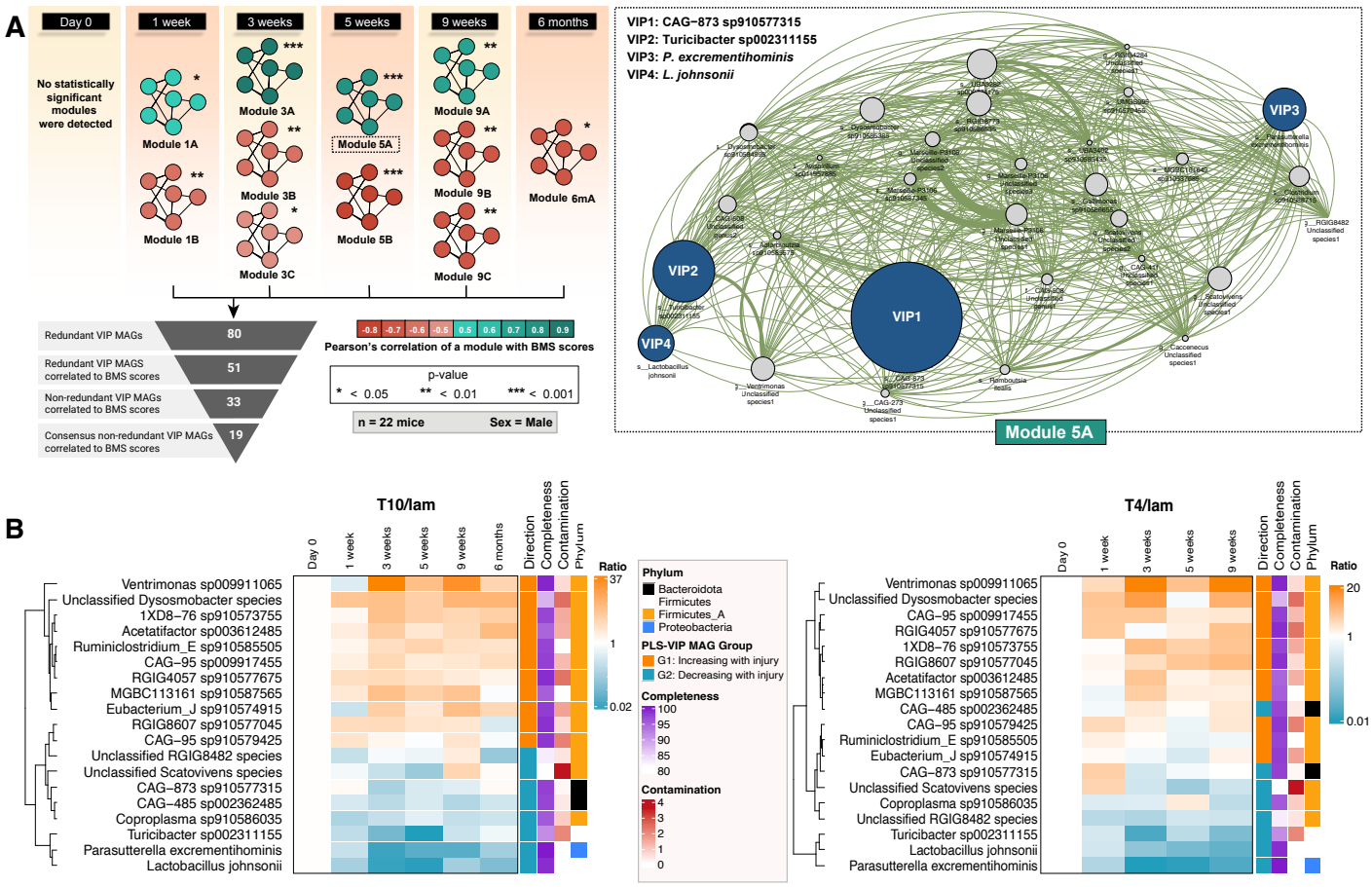

Fig. 1

Eco-systems biology distillation of interacting microbiota into host-impacting drivers.

(A) A schematic of statistically significant sub-communities (in shades of green and red) at each timepoint (see "*WGCNA Analysis*" in **Methods** and **Fig. S1** for details) correlated against 6-months-post-injury BMS score (colored for positive correlations and red for negative correlations and *p*-values as indicated). The modules (subnetworks) are named after the variable time-points: Module 1A = a module emerging at week 1, etc. The inverted pyramid (bottom) shows the number of MAGs filtered at each step of the workflow, distilled to 19 consensus MAGs after accounting for statistical anomalies and normal (i.e., Lam) microbiome drift over time (see "*Inspection of PLS-VIP MAGs*" in **Methods** for details). Inset (right) shows a network visualization of one module (i.e., subnetwork) at 5 weeks after surgery increasing with BMS score. All MAGs within

391 the module are shown in gray except for MAGs highlighted in blue whose VIP scores >=1 and
392 Pearson's correlation value with BMS score >=0.45. Node sizes are correlated with VIP scores
393 while edge widths are correlated with the strength of correlation between nodes (i.e., MAGs). This
394 module was visualized in Cytoscape v3.7.2. **(B-C)** Heatmaps temporally show the 19 consensus
395 PLS-VIP MAGs that change after NI at T10 and T4 spinal levels, respectively, compared to Lam.
396 The "Ratio" annotation column refers to the ratio of median fold change at an injury level divided
397 by median fold change at Lam to account for normal (i.e., Lam) microbiome drift over the course
398 of the study (see "*Fold-change calculation for visualizing the PLS-VIP MAGs*" in **Methods** for
399 details). G1: Group 1; G2: Group 2.

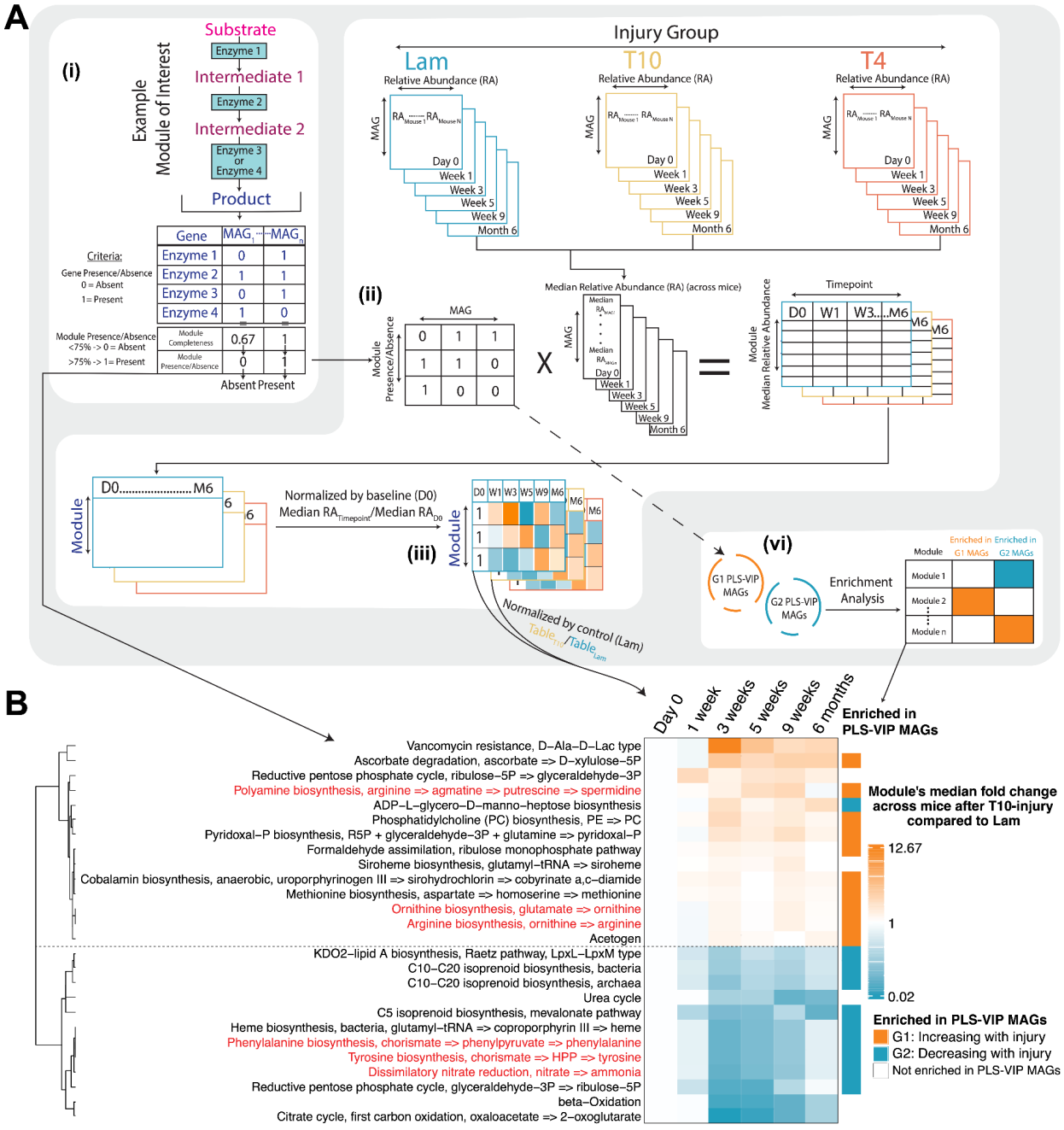

Fig. 2

Key metabolic pathways influenced by the spinal cord-gut axis.

(**A**) A schematic detailing the workflow developed to determine differentially abundant PLS-VIP MAGs-driven metabolic pathways, including (i) calculating presence/absence of each pathway (i.e., KEGG modules), (ii) integrating the MAG abundance data to calculate the median relative

406 abundance of each pathway, (iii) calculating the module's fold-change of median relative
407 abundance per injury and across injuries, and (iv) the functional enrichment analysis performed on
408 modules across the two groups of PLS-VIP MAGs. NI at T10 and T4 spinal levels, partially or
409 completely, disrupts neural control over the gut. **(B)** Heatmap representing differentially abundant
410 metabolic pathways at the community level (i.e., all de-replicated MAGs) and their enrichment in
411 the two groups of PLS-VIP MAGs caused by NI. Heatmap values indicate the ratio of median fold
412 changes at T10 divided by median fold change at Lam to account for normal (i.e., Lam)
413 microbiome drift over time in male mice (see "*Fold-change calculation for visualizing pathways*"
414 in **Methods** for more details and **Fig. S2-3** for the complete representation of all pathways
415 following T10 and T4 spinal lesions for male and female mice). Pathways annotated in orange are
416 enriched in PLS-VIP MAGs that increase after NI while those in teal are enriched in PLS-VIP
417 MAGs that decrease. Red text highlights pathways discussed in this report that are thought to be
418 involved in microbial nitrogen metabolism and host nitrogen balance. G1: Group 1; G2: Group 2.

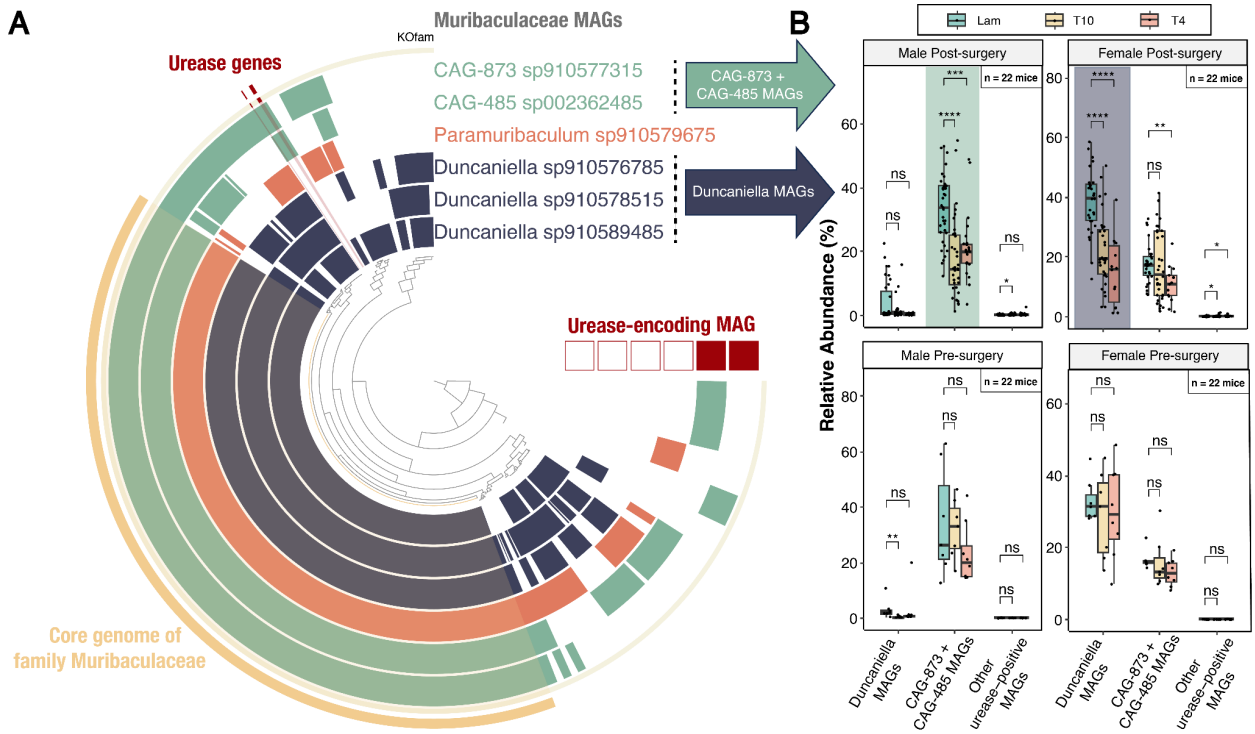

Fig. 3

Urease-encoding microbes influenced by the spinal cord-gut axis.

(**A**) Comparative genomics of urease-encoding MAGs within the Muribaculaceae family. MAGs belonging to the same genus are color-coded and MAGs encoding urease genes are indicated by filled red boxes. (**B**) Boxplots (with the 25th and 75th percentile ranges) of aggregate relative abundances of Muribaculaceae MAGs after (top) and before (bottom) NI in male and female mice. Peak changes are highlighted with color-shaded boxes for differentially abundant taxa in male (CAG-873 and CAG-485 MAGs) and female (Duncaniella MAGs) mice. Statistically significant differences in microbial relative abundances between treatments are indicated by the *p*-values from Wilcoxon tests. ****: $p <= 0.0001$, ***: $p <= 0.001$, **: $p <= 0.01$, *: $p <= 0.05$, ns: $p > 0.05$.

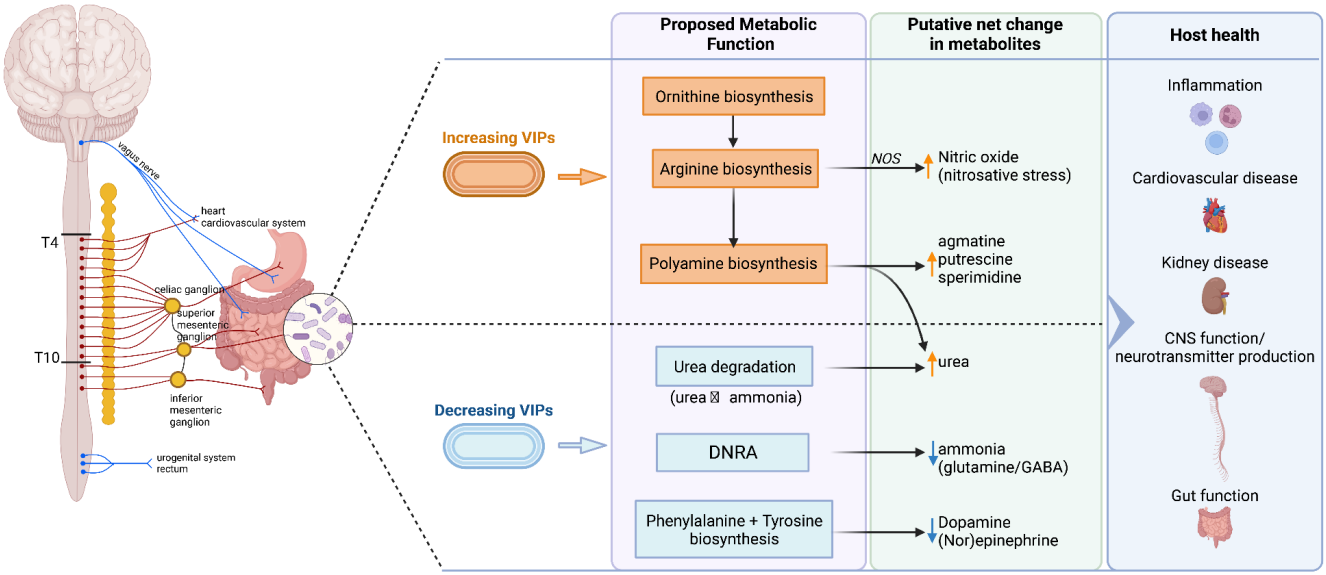

Fig. 4

Spinal cord-gut axis impacted microbiota metabolic pathways and their potential effects on host health.

Schematic of the spinal cord-gut axis and predicted metabolic functions associated with increasing or decreasing PLS-VIP MAGs following NI. For example (see main text for expanded discussions), PLS-VIP MAGs increasing in abundance (orange) following NI result in an increase in ornithine, arginine, and polyamine biosynthesis. These, in turn, can negatively affect host health via nitrosative stress (i.e., inflammation). Conversely, decreasing PLS-VIP MAGs alter ammonia and urea metabolisms, as well as phenylalanine and tyrosine biosynthesis. A reduction in these MAGs after NI could potentially affect neurotransmitter (e.g., dopaminergic, adrenergic, and GABAergic pathways) availability required for various CNS functions.

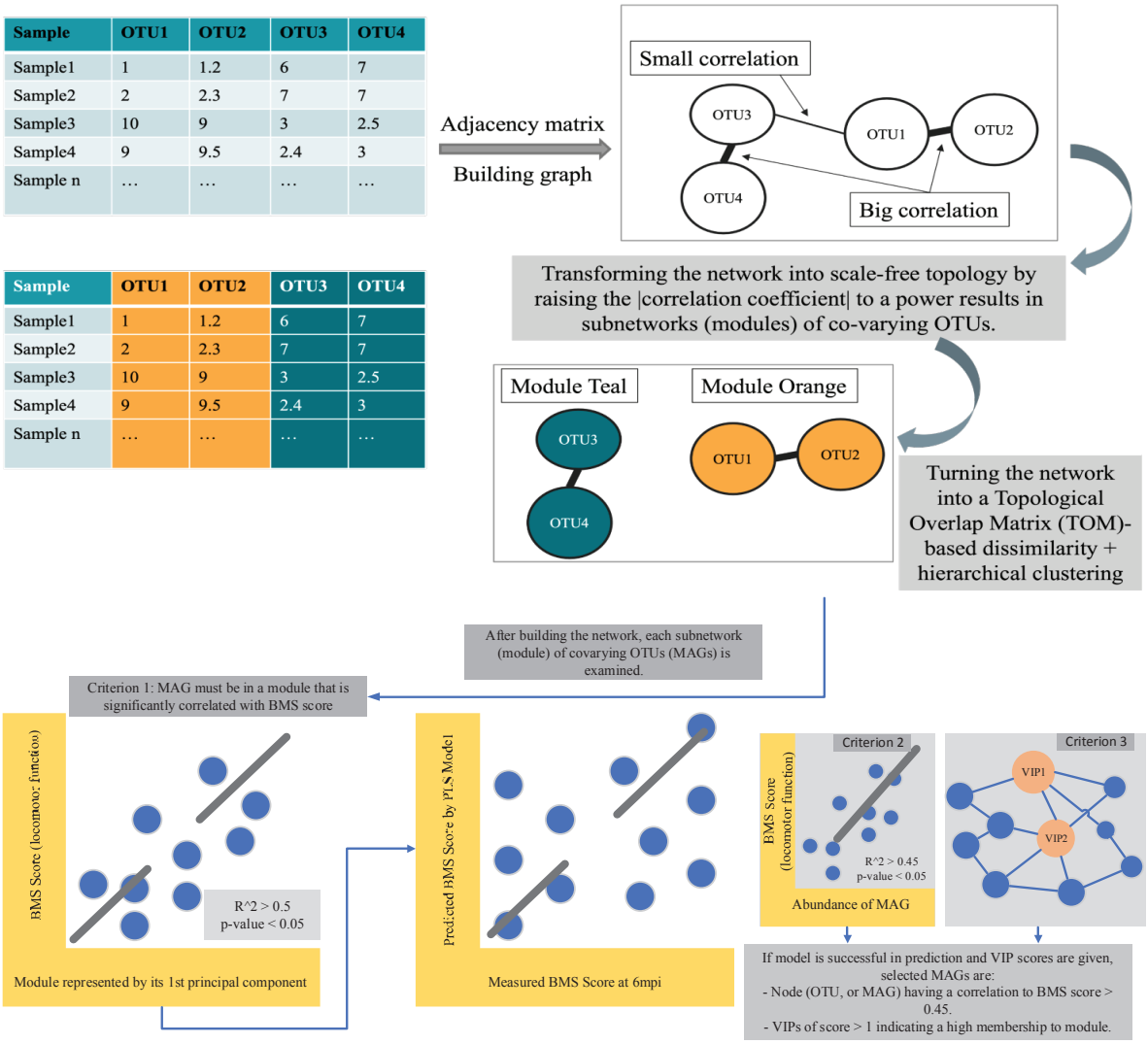

Fig. S1

Schematic showing WGCNA analysis to identify key MAGs relevant to neurological outcome after a break in spinal cord-gut communication.

MAG abundance-based correlation networks were built separately for male and female samples for each timepoint. The workflow summarizes the steps followed for each of these individual networks (see "*WGCNA Analysis*" in **Methods** for details). First, a graph was built from MAGs (as operational taxonomic units; OTUs) relative abundances and the edges in this network were iteratively transformed (by a power-law function) to meet the scale-free topology assumption for this network. Subnetworks (or modules) from each network were then identified and individually examined across three criteria to identify PLS-VIP MAGs. First, the subnetwork is significantly

454 correlated (correlation coefficient of >=|0.5|, p-value <0.05) to BMS score (as a marker of injury
455 severity). Second, cross-validated partial least squares (PLS) regression between measured and
456 predicted BMS scores for each subnetwork identified the MAG as a key taxon driving the change
457 in this subcommunity by the means of variable importance in projection (VIP) designation (VIP
458 score >= 1). Third, the PLS-VIP MAG is directly or inversely correlated to BMS score using a
459 standard correlation analysis (Pearson's correlation to BMS score >=|0.45|). Finally, consensus
460 PLS-VIP MAGs were further selected based on manual inspection of statistical anomalies and
461 normal (i.e., Lam) microbiome drift over time (see "*Inspection of PLS-VIP MAGs*" in **Methods**
462 for details).

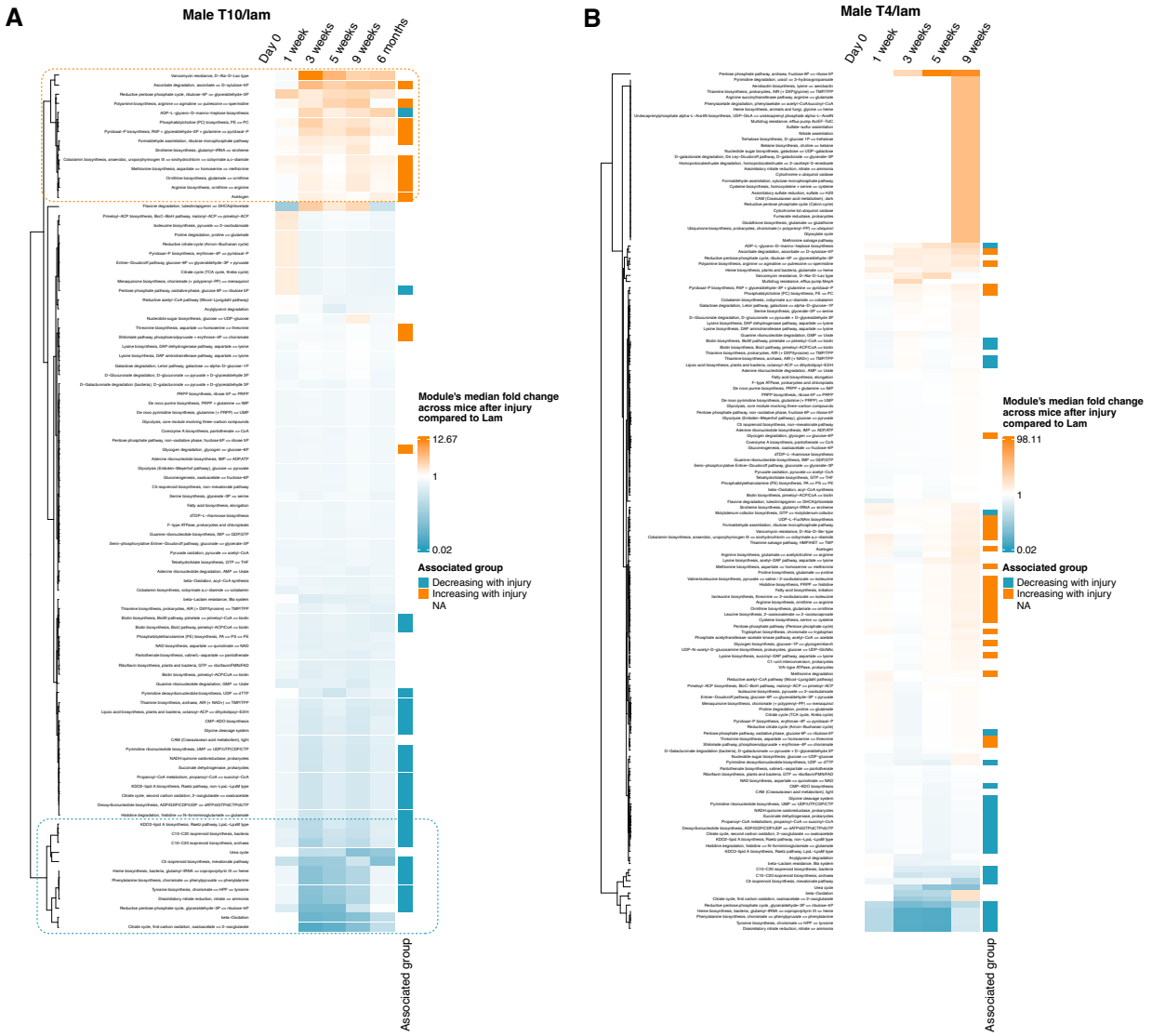

Fig. S2

Hierarchical clustering of KEGG pathway changes in male mice.

KEGG pathway changes were calculated across the entire community of MAGs to provide an estimate of the overall KEGG module change in the microbiome within injury groups (**A**, T10/lam; **B**, T4/lam) and at different timepoints. Heatmap values indicate the ratio of median fold changes at T10 (**A**) or T4 (**B**) divided by median fold change at Lam to account for normal (i.e., Lam) microbiome drift over time in male mice (see "*Fold-change calculation for visualizing pathways*" in **Methods** for more details). Pathways annotated in orange are enriched in PLS-VIP MAGs that increase after NI while those in teal are enriched in PLS-VIP MAGs that decrease. These modules

473 were compared with the VIP modules from **Fig. S4B** to identify "Community VIP-driven
474 modules" or cVIP-driven modules. The 26 modules within the top and bottom cluster of heatmap
475 (see boxed regions in panel A) are shown in **Fig. 2B**, which represent the highest changes in T10
476 (panel A) and encompass all changes in T10-T4 in male and female mice data (see **Fig. S3**).

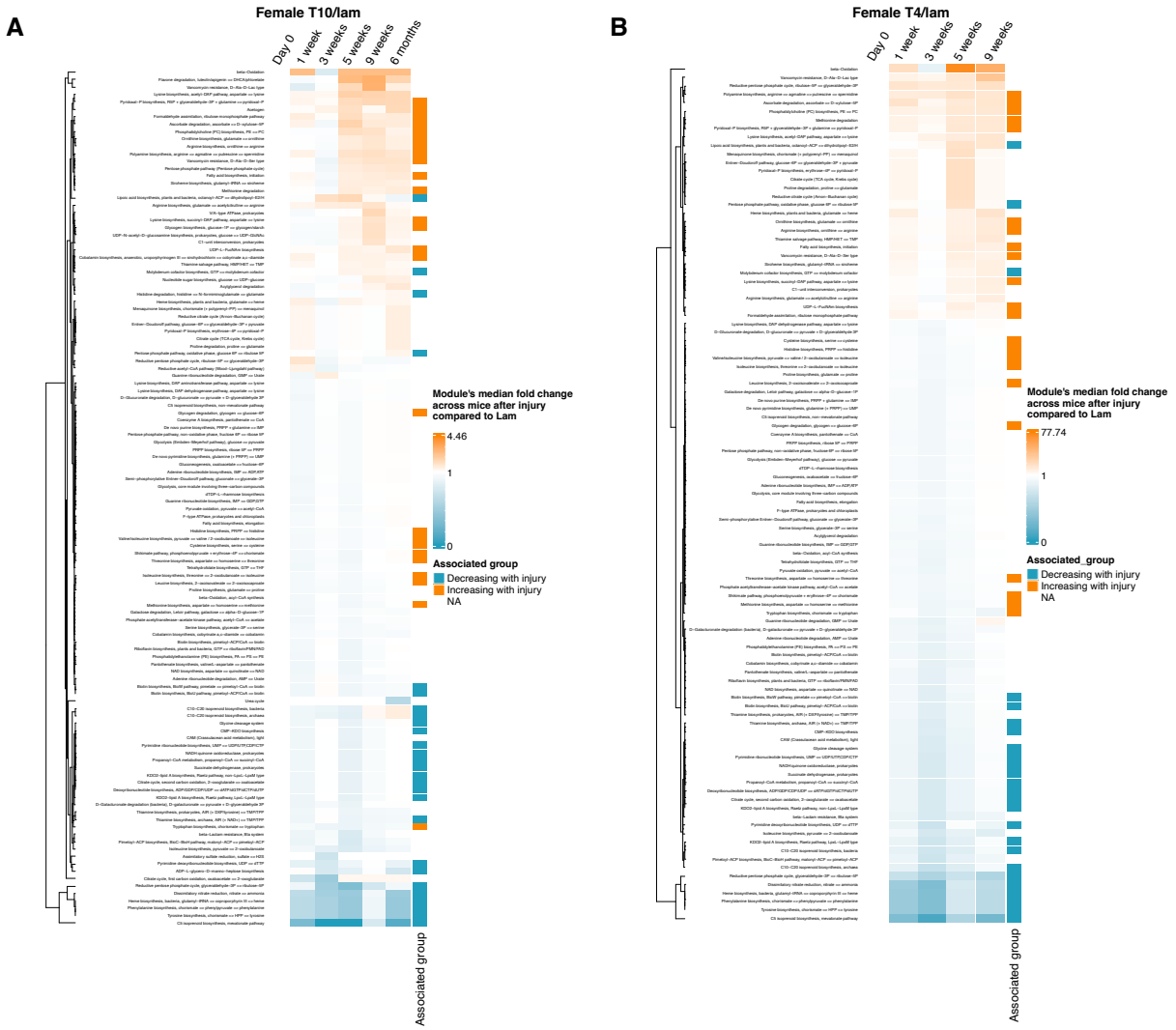

Fig. S3

Hierarchical clustering of KEGG pathway changes in female mice.

KEGG pathway changes were calculated across the entire community of MAGs to provide an estimate of the overall KEGG module change in the microbiome within injury groups (**A**, T10/lam; **B**, T4/lam) and at different timepoints. Heatmap values indicate the ratio of median fold changes at T10 (**A**) or T4 (**B**) divided by median fold change at Lam to account for normal (i.e., Lam) microbiome drift over time in female mice (see "*Fold-change calculation for visualizing pathways*" in **Methods** for more details). Pathways annotated in orange are enriched in PLS-VIP MAGs that increase after NI while those in teal are enriched in PLS-VIP MAGs that decrease.

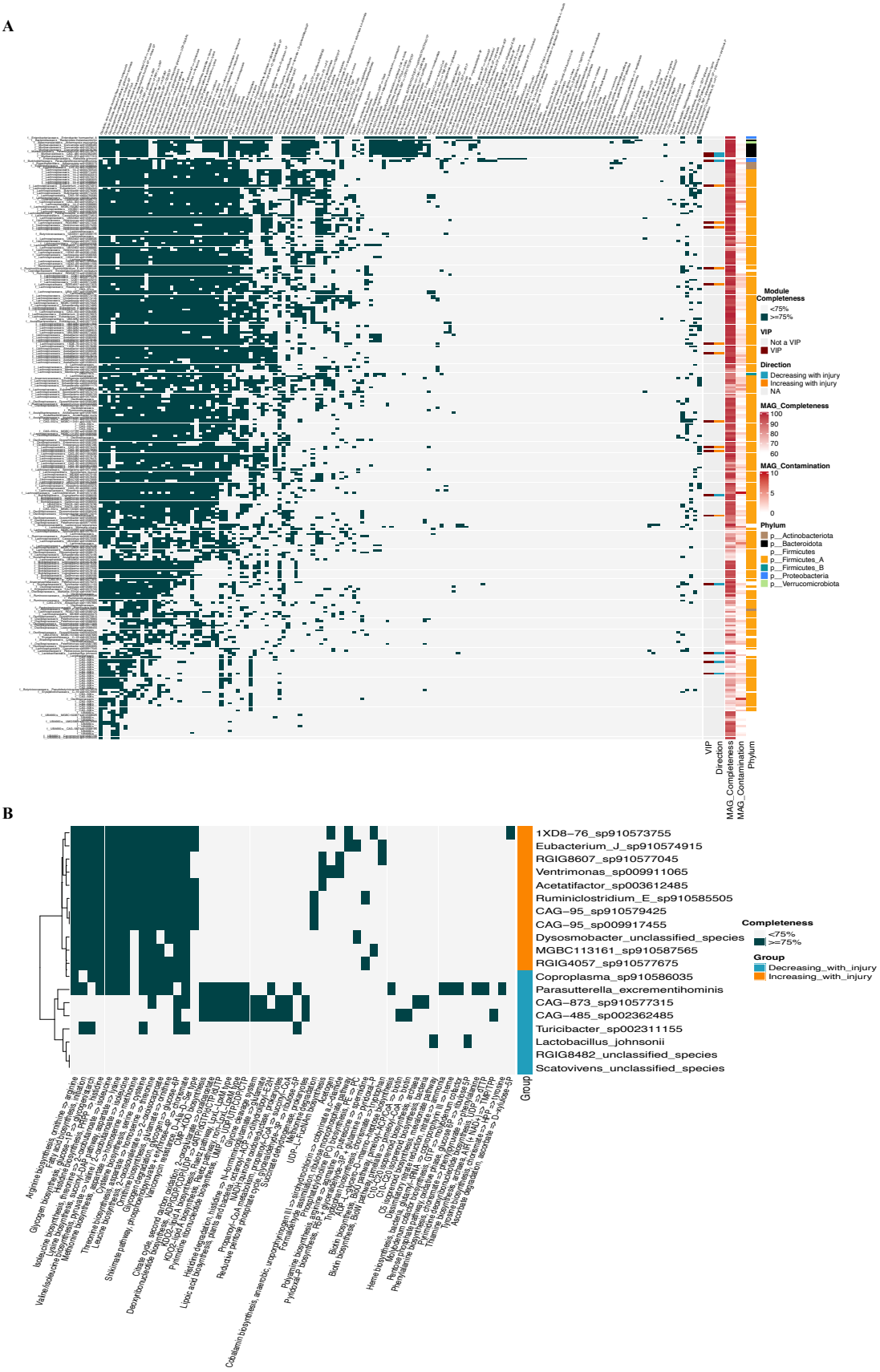
A
Module Completeness
<75%
>=75%
VIP
Not a VIP
VIP
Direction
Decreasing with injury
Increasing with injury
NA
MAG_Completeness
100
90
80
70
60
MAG_Contamination
10
5
0
Phylum
p__Actinobacteriota
p__Bacteroidota
p__Firmicutes
p__Firmicutes_A
p__Firmicutes_B
p__Proteobacteria
p__Verrucomicrobiota
VIP
Direction
MAG_Completeness
MAG_Contamination
Phylum
B
1XD8−76_sp910573755
Eubacterium_J_sp910574915
RGIG8607_sp910577045
Ventrimonas_sp009911065
Acetatifactor_sp003612485
Ruminiclostridium_E_sp910585505
CAG−95_sp910579425
CAG−95_sp009917455
Dysosmobacter_unclassified_species
MGBC113161_sp910587565
RGIG4057_sp910577675
Coproplasma_sp910586035
Parasutterella_excrementihominis
CAG−873_sp910577315
CAG−485_sp002362485
Turicibacter_sp002311155
Lactobacillus_johnsonii
RGIG8482_unclassified_species
Scatovivens_unclassified_species
Completeness
<75%
>=75%
Group
Decreasing_with_injury
Increasing_with_injury
Group

487

488 Fig. S4

489 **Heatmaps of KEGG modules presence-absence data of all MAGs and of PLS-VIP MAGs**
490 **that change after a break in gut-spinal cord communication.**

491 **(A)** KEGG modules encoded by all 263 de-replicated MAGs. MAGs are annotated with relevant
492 information (e.g., contamination, completeness, phylum, and whether it is a PLS-VIP MAG). **(B)**
493 Significantly enriched KEGG modules in one of the two groups of PLS-VIP MAGs (see "*Pathway*
494 *enrichment analysis with Anvi'o*" in **Methods**). For (**A-B**), a module is considered encoded by a
495 MAG if the MAG encodes 75% or more of the module's constituent genes.

Methods

Animals and spinal cord injury

All surgical and post-operative care procedures were performed in accordance with the Ohio State University Institutional Animal Care and Use Committee following protocol described in[24]. Briefly, n= 29 female C57BL/6 mice and n=30 male C57BL/6 mice from Jackson Laboratories (Bar Harbor, Maine) were used in this study. To prevent gut microbial cross-contamination due to co-habitation, all mice were single-housed. Mice were anesthetized with an intraperitoneal cocktail of ketamine (80 mg/kg)/xylazine (10 mg/kg) after which a partial laminectomy was performed at the fourth thoracic spine (T4) or the tenth thoracic spine (T10). In mice modeling SCI, modified #5 Dumont forceps were inserted laterally and held closed for 3 seconds to produce a complete crush spinal cord injury. In total, 20 mice received a complete crush at T4, 20 mice received a complete crush at T10, and 19 mice received laminectomy (Lam) only.

Fecal samples for metagenomic sequencing were aseptically collected pre-injury, 1-week, 2-weeks, 3-weeks, 5-weeks, 9-weeks, and 6-months post-injury, immediately frozen and stored at -80°C.

WGCNA analysis (i.e., to identify MAGs Relevant to spinal cord-gut cross-talk)

To identify key MAGs, or species, driving dysbiosis in the microbial community from a healthy state (i.e., Lam mice) to a diseased state (i.e., T10- or T4-injured mice), co-occurrence networks were built with hellinger-transformed MAG abundances using the "decostand" function from the R package "vegan" (https://github.com/vegandevs/vegan). These networks were built under the framework of WGCNA[86] (R package: https://cran.r-project.org/web/packages/WGCNA/index.html), a systems biology approach used to detect significant associations between genes or taxa and a system variable (BMS-score of mice at 6-months post injury in this study). This continuous variable accounts for incomplete injuries or partial crushing of the spinal cord rather than using a categorical

variable such as injury levels. Here, WGCNA was used on male and female cohorts separately, and one network was built per each timepoint. All codes used were deposited in the accompanying Zenodo repository.

For building networks: Hellinger-transformed abundance tables were used to build the networks using the biweight midcorrelation method (corType="bicor"). The values used as soft thresholds to ensure the networks' free-scale topology were 10, 12, 12, 14, 16, and 18 for pre-injury (i.e., baseline, or Day 0), 1 week, 3 weeks, 5 weeks, 9 weeks, and 6 months post-injury, respectively. The corresponding values for female mice data were 10, 12, 14, 14, 10, 14. Networks were built by the blockwiseModules function in the WGCNA package, requiring the "signed" option for both networkType and TOMType, and a minimum module size of 15.

Finding modules significantly correlated to BMS score: For each subnetwork, or module, of covarying MAGs extracted from each network (e.g. per timepoint in males), pairwise Pearson's correlation coefficients and their corresponding *p*-values were calculated between the module's first principal component and the BMS score. A module was considered significant if it has a correlation coefficient of |0.5| or larger and a *p*-value of less than 0.05. The modules with the highest correlation scores were examined further. These included two modules at 1 week, three at 3 weeks, two at 5 weeks, three at 9 weeks, and one at 6 months. No modules with significant correlation were found at Day 0, corroborating that there were no baseline pre-injury differences. All significant modules and their correlation coefficients and *p*-values are shown in **Fig. 1A**.

PLS-VIP MAGs selection: To identify taxa driving changes per module, we applied partial least squares (PLS) regression to determine the best predictors of BMS score. This was validated by a leave-one-out cross-validation method. All predictors per module were ranked according to their contribution in the PLS regression, which is known as their value importance in projection (VIP). MAGs with larger than |0.45| Pearson's correlation to BMS score that also had a VIP score larger than 1 were considered important for the PLS

prediction and were thus further investigated. We refer to these MAGs as "PLS-VIP MAGs" throughout the manuscript (or "VIPs" for short).

Inspection of PLS-VIP MAGs: To identify "consensus" PLS-VIP MAGs, each MAG was tested a) temporally within each treatment (i.e., injury levels) and b) across treatments per each timepoint, both using pairwise wilcoxon tests as described above. Unless otherwise stated (see full rationale for the selection criteria for each MAG in the accompanying Zenodo repository), PLS-VIP MAGs were kept in the "consensus" list if: a) their abundances significantly changed over time in T10 and/or T4 mice compared to baseline (Day0) when testing was constrained by treatment; and b) their abundances significantly changed between Lam (control) and T10 or Lam and T4 at one or more timepoints when testing was constrained by timepoint. In both testing strategies, trends in control samples (e.g., significant changes in Lam over time) and at baseline (e.g., significant changes in T10 or T4 compared to Lam at Day0) were used to inform exclusion from the consensus list.

Fold-change calculation for visualizing the PLS-VIP MAGs (Fig. 1B-C)

In each mouse, the MAG's relative abundance at each timepoint was divided by its relative abundance at Day 0 after introducing small pseudo-counts (both quantities were multiplied by 1000 and added to 1) to avoid division by zero. The median fold-changes across mice was calculated for each taxon per injury and timepoint. The median fold-changes in T10 or T4 were then divided over those in Lam for each taxon and then plotted. The heatmap was constructed with the ComplexHeatmap package[87] (https://github.com/jokergoo/ComplexHeatmap) and all values were log2-transformed to improve color ranges.

Anvi'o pathway identification

Using Anvi'o v7.1 (https://github.com/merenlab/anvio) and all de-replicated MAGs as external genomes, the following commands were used with their default

585 parameters on each MAG: anvi-gen-contigs-database, anvi-run-hmms, anvi-run-kegg-
586 kofams, and anvi-estimate-metabolism (with --kegg-output-modes modules, kofam_hits
587 and --matrix-format). This gives identified KEGG modules and KO hits per MAG as well
588 as module completeness and presence-absence matrices per MAG. The default value (75%)
589 for module completeness was used.
590
591 **Pathway enrichment analysis with Anvi'o**
592
593 Using Anvi'o v7.1 and the PLS-VIP MAGs as external genomes, the anvi-
594 compute-metabolic-enrichment function was used to compute enrichment in the 2 groups
595 of PLS-VIP MAGs (i.e., the ones enriched in T10 or T4 compared to Lam and the ones
596 enriched in Lam compared to these two injuries). KEGG modules with an adjusted q-value
597 of less than 0.05 or ones that are present in one group while absent in the other were
598 considered and plotted in **Fig. S4B**.
599
600 **Fold-change calculation for visualizing pathways** (Fig. 2B and Fig. S2-3)
601
602 The abundance of a KEGG module (i.e., pathway) was calculated from the total of
603 the abundances of the MAGs encoding it. First, the median abundance of each MAG across
604 all mice per sex, injury, and timepoint was calculated. Next, this median abundance was
605 multiplied by the presence-absence value of the KEGG Module (1 or zero) determined by
606 Anvi'o as explained above, where a module is considered present if it is at least 75%
607 complete. These quantities (median MAG abundance across mice belonging to the same
608 injury and timepoint, multiplied by the module's presence/absence value) were then
609 summed for all MAGs to give an estimate of the overall KEGG module's abundance per
610 sex, injury and timepoint. For each sex, these values at each timepoint, per injury, were
611 then divided by the values at Day0 to calculate the median fold change. Finally, T10 and
612 T4 values were divided by the corresponding Lam values. Heatmaps were constructed with
613 the ComplexHeatmap package and all values were log10-transformed to improve color
614 ranges.

Data availability

All data produced in this study are publicly available. Curated data and all used codes and databases can be found in the following Zenodo DOI: 10.5281/zenodo.15613780 (Unpublished - preview here).

Acknowledgements

We appreciate the help and support from all members of the Popovich and Sullivan laboratories, especially Natalie Solonenko, who participated in data sequencing, and Ami Fofana for her immense help with visual representations. We'd also like to acknowledge the Center of Microbiome Science, Ohio Supercomputer Center, and the Riffomonas educational resource[88]. This work is funded by a National Institutes of Neurological Disorders and Stroke R35 award (grant no. 1R35NS111582) to P.G.P., The Belford Center for Spinal Cord Injury (P.G.P.), The Ray W. Poppleton Research designated endowment (P.G.P.), a Craig H. Nielsen Foundation Senior Research award (grant no. 890085) to K.A.K, and NSF awards ABI#2149505 and DBI#2022070 to M.B.S.

Author Contributions

P.G.P., M.B.S., K.A.K., A.A.Z. conceived the project and experimental design. P.G.P., M.B.S., K.A.K., A.A.Z., and M.M. developed the data analysis plan. P.G.P., M.B.S., K.A.K., A.A.Z., M.M., G.J.S., J.D., and J.M.S. helped with data interpretation and writing of the manuscript. M.M. performed the statistical, functional, bioinformatic, and eco-systems biology analyses, and managed and coordinated responsibilities for the manuscript preparation. A.A.Z. guided and supervised statistical, functional, and bioinformatic analyses, performed eco-systems biology analyses, co-developed the WGCNA pipeline, and drafted the manuscript with M.M.. M.M., K.A.K., A.A.Z., and G.J.S. contributed to figure generation and, with P.G.P., contributed to

improving illustrations. G.J.S. guided functional analyses. All authors read and reviewed the manuscript and approved it in its final form.

Declaration of interests

All authors declare no competing interest.

Declaration of generative AI and AI-assisted technologies

During preparation of this work, Microsoft CoPilot and ChatGPT were used periodically to improve writing or shorten passages. After using it, the authors reviewed and edited the content as needed and take full responsibility for the content of the publication.

REFERENCES

1. Moran, M.A., Kujawinski, E.B., Schroer, W.F., Amin, S.A., Bates, N.R., Bertrand, E.M., Braakman, R., Brown, C.T., Covert, M.W., Doney, S.C., et al. (2022). Microbial metabolites in the marine carbon cycle. Nat Microbiol *7*, 508–523. https://doi.org/10.1038/s41564-022-01090-3.

2. Schimel, J.P., and Schaeffer, S.M. (2012). Microbial control over carbon cycling in soil. Front Microbiol *3*, 348. https://doi.org/10.3389/fmicb.2012.00348.

3. Kuypers, M.M.M., Marchant, H.K., and Kartal, B. (2018). The microbial nitrogen-cycling network. Nat Rev Microbiol *16*, 263–276. https://doi.org/10.1038/nrmicro.2018.9.

4. Malard, L.A., and Guisan, A. (2023). Into the microbial niche. Trends Ecol Evol *38*, 936–945. https://doi.org/10.1016/j.tree.2023.04.015.

663 5. Valido, E., Bertolo, A., Fränkl, G.P., Itodo, O.A., Pinheiro, T., Pannek, J., Kopp-Heim, D.,
664 Glisic, M., and Stoyanov, J. (2022). Systematic review of the changes in the microbiome
665 following spinal cord injury: animal and human evidence. Spinal Cord *60*, 288–300.
666 https://doi.org/10.1038/s41393-021-00737-y.

667 6. Hou, K., Wu, Z.-X., Chen, X.-Y., Wang, J.-Q., Zhang, D., Xiao, C., Zhu, D., Koya, J.B., Wei,
668 L., Li, J., et al. (2022). Microbiota in health and diseases. Signal Transduct Target Ther *7*,
669 135. https://doi.org/10.1038/s41392-022-00974-4.

670 7. Sorboni, S.G., Moghaddam, H.S., Jafarzadeh-Esfehani, R., and Soleimanpour, S.
671 (2022). A Comprehensive Review on the Role of the Gut Microbiome in Human
672 Neurological Disorders. Clin Microbiol Rev *35*, e0033820.
673 https://doi.org/10.1128/CMR.00338-20.

674 8. Gohl, D.M., Vangay, P., Garbe, J., MacLean, A., Hauge, A., Becker, A., Gould, T.J.,
675 Clayton, J.B., Johnson, T.J., Hunter, R., et al. (2016). Systematic improvement of
676 amplicon marker gene methods for increased accuracy in microbiome studies. Nat
677 Biotechnol *34*, 942–949. https://doi.org/10.1038/nbt.3601.

678 9. Bonk, F., Popp, D., Harms, H., and Centler, F. (2018). PCR-based quantification of taxa-
679 specific abundances in microbial communities: Quantifying and avoiding common
680 pitfalls. J Microbiol Methods *153*, 139–147.
681 https://doi.org/10.1016/j.mimet.2018.09.015.

682 10. Coleman, M.L., and Chisholm, S.W. (2007). Code and context: Prochlorococcus as a
683 model for cross-scale biology. Trends Microbiol *15*, 398–407.
684 https://doi.org/10.1016/j.tim.2007.07.001.

685 11. Lesker, T.R., Durairaj, A.C., Gálvez, E.J.C., Lagkouvardos, I., Baines, J.F., Clavel, T.,
686 Sczyrba, A., McHardy, A.C., and Strowig, T. (2020). An Integrated Metagenome Catalog
687 Reveals New Insights into the Murine Gut Microbiome. Cell Rep *30*, 2909-2922.e6.
688 https://doi.org/10.1016/j.celrep.2020.02.036.

12. Arevalo, P., VanInsberghe, D., Elsherbini, J., Gore, J., and Polz, M.F. (2019). A Reverse Ecology Approach Based on a Biological Definition of Microbial Populations. Cell *178*, 820-834.e14. https://doi.org/10.1016/j.cell.2019.06.033.

13. Kim, N., Ma, J., Kim, W., Kim, J., Belenky, P., and Lee, I. (2024). Genome-resolved metagenomics: a game changer for microbiome medicine. Exp Mol Med *56*, 1501–1512. https://doi.org/10.1038/s12276-024-01262-7.

14. Eren, A.M., and Banfield, J.F. (2024). Modern microbiology: Embracing complexity through integration across scales. Cell *187*, 5151–5170. https://doi.org/10.1016/j.cell.2024.08.028.

15. Lynch, J.B., and Hsiao, E.Y. (2023). Toward understanding links between the microbiome and neurotransmitters. Annals of the New York Academy of Sciences *1524*, 10–16. https://doi.org/10.1111/nyas.14993.

16. Özçam, M., and Lynch, S.V. (2024). The gut–airway microbiome axis in health and respiratory diseases. Nat Rev Microbiol *22*, 492–506. https://doi.org/10.1038/s41579-024-01048-8.

17. Gilbert, J.A., Azad, M.B., Bäckhed, F., Blaser, M.J., Byndloss, M., Chiu, C.Y., Chu, H., Dugas, L.R., Elinav, E., Gibbons, S.M., et al. (2025). Clinical translation of microbiome research. Nat Med *31*, 1099–1113. https://doi.org/10.1038/s41591-025-03615-9.

18. Chen, L., Collij, V., Jaeger, M., van den Munckhof, I.C.L., Vich Vila, A., Kurilshikov, A., Gacesa, R., Sinha, T., Oosting, M., Joosten, L.A.B., et al. (2020). Gut microbial co-abundance networks show specificity in inflammatory bowel disease and obesity. Nat Commun *11*, 4018. https://doi.org/10.1038/s41467-020-17840-y.

19. Bäumler, A.J., and Sperandio, V. (2016). Interactions between the microbiota and pathogenic bacteria in the gut. Nature *535*, 85–93. https://doi.org/10.1038/nature18849.

714 20. Human Microbiome Project Consortium (2012). Structure, function and diversity of the
715 healthy human microbiome. Nature *486*, 207–214.
716 https://doi.org/10.1038/nature11234.

717 21. Martín, R., Rios-Covian, D., Huillet, E., Auger, S., Khazaal, S., Bermúdez-Humarán,
718 L.G., Sokol, H., Chatel, J.-M., and Langella, P. (2023). Faecalibacterium: a bacterial
719 genus with promising human health applications. FEMS Microbiol Rev *47*, fuad039.
720 https://doi.org/10.1093/femsre/fuad039.

721 22. Lin, N.Y.-T., Fukuoka, S., Koyama, S., Motooka, D., Tourlousse, D.M., Shigeno, Y.,
722 Matsumoto, Y., Yamano, H., Murotomi, K., Tamaki, H., et al. (2025). Microbiota-driven
723 antitumour immunity mediated by dendritic cell migration. Nature.
724 https://doi.org/10.1038/s41586-025-09249-8.

725 23. Kumar, S., Mukherjee, R., Gaur, P., Leal, É., Lyu, X., Ahmad, S., Puri, P., Chang, C.-M.,
726 Raj, V.S., and Pandey, R.P. (2025). Unveiling roles of beneficial gut bacteria and optimal
727 diets for health. Front Microbiol *16*, 1527755.
728 https://doi.org/10.3389/fmicb.2025.1527755.

729 24. Mohssen, M., Zayed, A.A., Kigerl, K.A., Du, J., Smith, G.J., Schwab, J.M., Sullivan, M.B.,
730 and Popovich, P.G. (2025). Disruption of The Spinal Cord-Gut Axis Alters Gut Microbial
731 Dynamics and Carbohydrate Cross-feeding. bioRxiv, 2025.05.27.656368.
732 https://doi.org/10.1101/2025.05.27.656368.

733 25. Sonnenburg, J.L., Chen, C.T.L., and Gordon, J.I. (2006). Genomic and metabolic studies
734 of the impact of probiotics on a model gut symbiont and host. PLoS Biol *4*, e413.
735 https://doi.org/10.1371/journal.pbio.0040413.

736 26. Sunagawa, S., Acinas, S.G., Bork, P., Bowler, C., Eveillard, D., Gorsky, G., Guidi, L.,
737 Iudicone, D., Karsenti, E., Lombard, F., et al. (2020). Tara Oceans: towards global
738 ocean ecosystems biology. Nat Rev Microbiol *18*, 428–445.
739 https://doi.org/10.1038/s41579-020-0364-5.

740 27. Lorenzi, R.M., Palesi, F., Castellazzi, G., Vitali, P., Anzalone, N., Bernini, S., Cotta
741 Ramusino, M., Sinforiani, E., Micieli, G., Costa, A., et al. (2020). Unsuspected
742 Involvement of Spinal Cord in Alzheimer Disease. Front Cell Neurosci *14*, 6.
743 https://doi.org/10.3389/fncel.2020.00006.

744 28. Emmenegger, T.M., Seiler, R., Unschuld, P.G., Freund, P., Klohs, J., and Alzheimer's
745 Disease Neuroimaging Initiative (2024). Progressive cervical cord atrophy parallels
746 cognitive decline in Alzheimer's disease. Sci Rep *14*, 21595.
747 https://doi.org/10.1038/s41598-024-67389-9.

748 29. Del Tredici, K., and Braak, H. (2012). Spinal cord lesions in sporadic Parkinson's
749 disease. Acta Neuropathol *124*, 643–664. https://doi.org/10.1007/s00401-012-1028-y.

750 30. Kreiter, D., Postma, A.A., Hupperts, R., and Gerlach, O. (2024). Hallmarks of spinal
751 cord pathology in multiple sclerosis. J Neurol Sci *456*, 122846.
752 https://doi.org/10.1016/j.jns.2023.122846.

753 31. Saberi, S., Stauffer, J.E., Schulte, D.J., and Ravits, J. (2015). Neuropathology of
754 Amyotrophic Lateral Sclerosis and Its Variants. Neurol Clin *33*, 855–876.
755 https://doi.org/10.1016/j.ncl.2015.07.012.

756 32. Karbasforoushan, H., Cohen-Adad, J., and Dewald, J.P.A. (2019). Brainstem and spinal
757 cord MRI identifies altered sensorimotor pathways post-stroke. Nat Commun *10*, 3524.
758 https://doi.org/10.1038/s41467-019-11244-3.

759 33. Irvine, K.-A., Sahbaie, P., Liang, D.-Y., and Clark, J.D. (2018). Traumatic Brain Injury
760 Disrupts Pain Signaling in the Brainstem and Spinal Cord. J Neurotrauma *35*, 1495–
761 1509. https://doi.org/10.1089/neu.2017.5411.

762 34. Du, J., Zayed, A.A., Kigerl, K.A., Zane, K., Sullivan, M.B., and Popovich, P.G. Spinal Cord
763 Injury Changes the Structure and Functional Potential of Gut Bacterial and Viral
764 Communities. mSystems *6*, e01356-20. https://doi.org/10.1128/mSystems.01356-20.

765 35. Dionyssiotis, Y., Papachristos, A., Petropoulou, K., Papathanasiou, J., and
766 Papagelopoulos, P. (2016). Nutritional Alterations Associated with Neurological and
767 Neurosurgical Diseases. Open Neurol J *10*, 32–41.
768 https://doi.org/10.2174/1874205X01610010032.

769 36. Kim, T.J., Park, S.-H., Jeong, H.-B., Ha, E.J., Cho, W.S., Kang, H.-S., Kim, J.E., and Ko, S.-
770 B. (2020). Optimizing Nitrogen Balance Is Associated with Better Outcomes in
771 Neurocritically Ill Patients. Nutrients *12*, 3137. https://doi.org/10.3390/nu12103137.

772 37. Guidi, L., Chaffron, S., Bittner, L., Eveillard, D., Larhlimi, A., Roux, S., Darzi, Y., Audic,
773 S., Berline, L., Brum, J.R., et al. (2016). Plankton networks driving carbon export in the
774 oligotrophic ocean. Nature *532*, 465–470. https://doi.org/10.1038/nature16942.

775 38. Zhang, B., and Horvath, S. (2005). A general framework for weighted gene co-
776 expression network analysis. Stat Appl Genet Mol Biol *4*, Article17.
777 https://doi.org/10.2202/1544-6115.1128.

778 39. Bai, Y., Lyu, M., Fukunaga, M., Watanabe, S., Iwatani, S., Miyanaga, K., and Yamamoto,
779 N. (2022). Lactobacillus johnsonii enhances the gut barrier integrity via the interaction
780 between GAPDH and the mouse tight junction protein JAM-2. Food Funct *13*, 11021–
781 11033. https://doi.org/10.1039/d2fo00886f.

782 40. Jia, D.-J.-C., Wang, Q.-W., Hu, Y.-Y., He, J.-M., Ge, Q.-W., Qi, Y.-D., Chen, L.-Y., Zhang,
783 Y., Fan, L.-N., Lin, Y.-F., et al. (2022). Lactobacillus johnsonii alleviates colitis by
784 TLR1/2-STAT3 mediated CD206+ macrophagesIL-10 activation. Gut Microbes *14*,
785 2145843. https://doi.org/10.1080/19490976.2022.2145843.

786 41. Zhu, H., Zhao, F., Zhang, W., Xia, W., Chen, Y., Liu, Y., Fan, Z., Zhang, Y., and Yang, Y.
787 (2022). Cholesterol-lowering effect of bile salt hydrolase from a Lactobacillus johnsonii
788 strain mediated by FXR pathway regulation. Food Funct *13*, 725–736.
789 https://doi.org/10.1039/d1fo03143k.

790 42. Feng, C., Li, N., Gao, G., He, Q., Kwok, L.-Y., and Zhang, H. (2024). Dynamic Changes of
791 the Gut Microbiota and Its Functional Metagenomic Potential during the Development
792 of Non-Small Cell Lung Cancer. Int J Mol Sci *25*, 3768.
793 https://doi.org/10.3390/ijms25073768.

794 43. Lynch, J.B., Gonzalez, E.L., Choy, K., Faull, K.F., Jewell, T., Arellano, A., Liang, J., Yu,
795 K.B., Paramo, J., and Hsiao, E.Y. (2023). Gut microbiota Turicibacter strains
796 differentially modify bile acids and host lipids. Nat Commun *14*, 3669.
797 https://doi.org/10.1038/s41467-023-39403-7.

798 44. Ju, T., Kong, J.Y., Stothard, P., and Willing, B.P. (2019). Defining the role of
799 Parasutterella, a previously uncharacterized member of the core gut microbiota. ISME J
800 *13*, 1520–1534. https://doi.org/10.1038/s41396-019-0364-5.

801 45. Forster, S.C., Clare, S., Beresford-Jones, B.S., Harcourt, K., Notley, G., Stares, M.D.,
802 Kumar, N., Soderholm, A.T., Adoum, A., Wong, H., et al. (2022). Identification of gut
803 microbial species linked with disease variability in a widely used mouse model of
804 colitis. Nat Microbiol *7*, 590–599. https://doi.org/10.1038/s41564-022-01094-z.

805 46. Künstner, A., Schilf, P., Busch, H., Ibrahim, S.M., and Hirose, M. (2022). Changes of Gut
806 Microbiota by Natural mtDNA Variant Differences Augment Susceptibility to Metabolic
807 Disease and Ageing. Int J Mol Sci *23*, 1056. https://doi.org/10.3390/ijms23031056.

808 47. Saravi, S.S.S., Pugin, B., Constancias, F., Thomas, A., Gludic, S.L., Allemann, M.S.,
809 Karsai, G., Lee, P., Menni, C., Attaye, I., et al. (2023). Gut microbiota-dependent
810 increase in phenylacetic acid induces endothelial cell senescence during aging.
811 Preprint at bioRxiv, https://doi.org/10.1101/2023.11.17.567594
812 https://doi.org/10.1101/2023.11.17.567594.

813 48. Culp, E.J., and Goodman, A.L. (2023). Cross-feeding in the gut microbiome: Ecology
814 and mechanisms. Cell Host Microbe *31*, 485–499.
815 https://doi.org/10.1016/j.chom.2023.03.016.

816 49. Eren, A.M., Kiefl, E., Shaiber, A., Veseli, I., Miller, S.E., Schechter, M.S., Fink, I., Pan,
817 J.N., Yousef, M., Fogarty, E.C., et al. (2021). Community-led, integrated, reproducible
818 multi-omics with anvi'o. Nat Microbiol *6*, 3–6. https://doi.org/10.1038/s41564-020-
819 00834-3.

820 50. Veseli, I., Chen, Y.T., Schechter, M.S., Vanni, C., Fogarty, E.C., Watson, A.R., Jabri, B.A.,
821 Blekhman, R., Willis, A.D., Yu, M.K., et al. (2024). Microbes with higher metabolic
822 independence are enriched in human gut microbiomes under stress. bioRxiv,
823 2023.05.10.540289. https://doi.org/10.1101/2023.05.10.540289.

824 51. Shaiber, A., Willis, A.D., Delmont, T.O., Roux, S., Chen, L.-X., Schmid, A.C., Yousef, M.,
825 Watson, A.R., Lolans, K., Esen, Ö.C., et al. (2020). Functional and genetic markers of
826 niche partitioning among enigmatic members of the human oral microbiome. Genome
827 Biol *21*, 292. https://doi.org/10.1186/s13059-020-02195-w.

828 52. Kraft, B., Strous, M., and Tegetmeyer, H.E. (2011). Microbial nitrate respiration – Genes,
829 enzymes and environmental distribution. Journal of Biotechnology *155*, 104–117.
830 https://doi.org/10.1016/j.jbiotec.2010.12.025.

831 53. Jones, G.A. (1972). Dissimilatory metabolism of nitrate by the rumen microbiota. Can J
832 Microbiol *18*, 1783–1787. https://doi.org/10.1139/m72-279.

833 54. Allison, C., and Macfarlane, G.T. (1988). Effect of nitrate on methane production and
834 fermentation by slurries of human faecal bacteria. J Gen Microbiol *134*, 1397–1405.
835 https://doi.org/10.1099/00221287-134-6-1397.

836 55. The Dissimilatory Reduction of Nitrate to Ammonia by Anaerobic Bacteria -
837 ScienceDirect
838 https://www.sciencedirect.com/science/article/abs/pii/B9780444528575500084?via
839 %3Dihub.

840 56. Vermeiren, J., Van de Wiele, T., Verstraete, W., Boeckx, P., and Boon, N. (2009). Nitric
841 oxide production by the human intestinal microbiota by dissimilatory nitrate reduction
842 to ammonium. J Biomed Biotechnol *2009*, 284718.
843 https://doi.org/10.1155/2009/284718.

844 57. Fuller, M.F., and Reeds, P.J. (1998). Nitrogen cycling in the gut. Annu Rev Nutr *18*, 385–
845 411. https://doi.org/10.1146/annurev.nutr.18.1.385.

846 58. Stewart, G.S., and Smith, C.P. (2005). Urea nitrogen salvage mechanisms and their
847 relevance to ruminants, non-ruminants and man. Nutr Res Rev *18*, 49–62.
848 https://doi.org/10.1079/NRR200498.

849 59. Wang, P., Wu, P.-F., Wang, H.-J., Liao, F., Wang, F., and Chen, J.-G. (2023). Gut
850 microbiome-derived ammonia modulates stress vulnerability in the host. Nat Metab *5*,
851 1986–2001. https://doi.org/10.1038/s42255-023-00909-5.

852 60. Douglas, G.M., Maffei, V.J., Zaneveld, J.R., Yurgel, S.N., Brown, J.R., Taylor, C.M.,
853 Huttenhower, C., and Langille, M.G.I. (2020). PICRUSt2 for prediction of metagenome
854 functions. Nat Biotechnol *38*, 685–688. https://doi.org/10.1038/s41587-020-0548-6.

855 61. Carr, A., Diener, C., Baliga, N.S., and Gibbons, S.M. (2019). Use and abuse of
856 correlation analyses in microbial ecology. ISME J *13*, 2647–2655.
857 https://doi.org/10.1038/s41396-019-0459-z.

858 62. Fischbach, M.A., and Sonnenburg, J.L. (2011). Eating for two: how metabolism
859 establishes interspecies interactions in the gut. Cell Host Microbe *10*, 336–347.
860 https://doi.org/10.1016/j.chom.2011.10.002.

861 63. Assessment of sex differences in serum urea and creatinine levels following an acute
862 spinal cord injury in albino rat models | Bayero Journal of Medical Laboratory Science
863 https://www.ajol.info/index.php/bjmls/article/view/222018.

64. Rodriguez, D.J., Clevenger, F.W., Osler, T.M., Demarest, G.B., and Fry, D.E. (1991). Obligatory negative nitrogen balance following spinal cord injury. JPEN J Parenter Enteral Nutr *15*, 319–322. https://doi.org/10.1177/0148607191015003319.

65. Thibault-Halman, G., Casha, S., Singer, S., and Christie, S. (2011). Acute management of nutritional demands after spinal cord injury. J Neurotrauma *28*, 1497–1507. https://doi.org/10.1089/neu.2009.1155.

66. Harris, A.N., Lee, H.-W., Osis, G., Fang, L., Webster, K.L., Verlander, J.W., and Weiner, I.D. (2018). Differences in renal ammonia metabolism in male and female kidney. Am J Physiol Renal Physiol *315*, F211–F222. https://doi.org/10.1152/ajprenal.00084.2018.

67. Harris, A.N., Castro, R.A., Lee, H.-W., Verlander, J.W., and Weiner, I.D. (2021). Role of the renal androgen receptor in sex differences in ammonia metabolism. Am J Physiol Renal Physiol *321*, F629–F644. https://doi.org/10.1152/ajprenal.00260.2021.

68. Mora, D., and Arioli, S. (2014). Microbial Urease in Health and Disease. PLoS Pathog *10*, e1004472. https://doi.org/10.1371/journal.ppat.1004472.

69. Gonzalez-Lopez, E., and Vrana, K.E. (2020). Dopamine beta-hydroxylase and its genetic variants in human health and disease. J Neurochem *152*, 157–181. https://doi.org/10.1111/jnc.14893.

70. Wu, G., and Morris, S.M. (1998). Arginine metabolism: nitric oxide and beyond. Biochem J *336 (Pt 1)*, 1–17. https://doi.org/10.1042/bj3360001.

71. McRae, M.P. (2016). Therapeutic Benefits of l-Arginine: An Umbrella Review of Meta-analyses. J Chiropr Med *15*, 184–189. https://doi.org/10.1016/j.jcm.2016.06.002.

72. Kasahara, N., Teratani, T., Yokota, S., Sakuma, Y., Sasanuma, H., Fujimoto, Y., Ijichi, T., Urahashi, T., Yoshitomi, H., Kitayama, J., et al. (2024). Dietary polyamines promote

887 intestinal adaptation in an experimental model of short bowel syndrome. Sci Rep *14*,
888 4605. https://doi.org/10.1038/s41598-024-55258-4.

889 73. Erens, C., Van Broeckhoven, J., Hoeks, C., Schabbauer, G., Cheng, P.N., Chen, L.,
890 Hellings, N., Broux, B., Lemmens, S., and Hendrix, S. (2022). L-Arginine Depletion
891 Improves Spinal Cord Injury via Immunomodulation and Nitric Oxide Reduction.
892 Biomedicines *10*, 205. https://doi.org/10.3390/biomedicines10020205.

893 74. Erens, C., Van Broeckhoven, J., Bronckaers, A., Lemmens, S., and Hendrix, S. (2023).
894 The Dark Side of an Essential Amino Acid: L-Arginine in Spinal Cord Injury. J
895 Neurotrauma *40*, 820–832. https://doi.org/10.1089/neu.2022.0271.

896 75. Saito, A., Takagi, T., Chung, T.G., and Ohta, K. (1983). Serum levels of polyamines in
897 patients with chronic renal failure. Kidney Int Suppl *16*, S234-237.

898 76. Piletz, J.E., Aricioglu, F., Cheng, J.-T., Fairbanks, C.A., Gilad, V.H., Haenisch, B.,
899 Halaris, A., Hong, S., Lee, J.E., Li, J., et al. (2013). Agmatine: clinical applications after
900 100 years in translation. Drug Discov Today *18*, 880–893.
901 https://doi.org/10.1016/j.drudis.2013.05.017.

902 77. Saha, P., Panda, S., Holkar, A., Vashishth, R., Rana, S.S., Arumugam, M., Ashraf, G.M.,
903 Haque, S., and Ahmad, F. (2023). Neuroprotection by agmatine: Possible involvement
904 of the gut microbiome? Ageing Research Reviews *91*, 102056.
905 https://doi.org/10.1016/j.arr.2023.102056.

906 78. Beresford-Jones, B.S., Forster, S.C., Stares, M.D., Notley, G., Viciani, E., Browne, H.P.,
907 Boehmler, D.J., Soderholm, A.T., Kumar, N., Vervier, K., et al. (2022). The Mouse
908 Gastrointestinal Bacteria Catalogue enables translation between the mouse and
909 human gut microbiotas via functional mapping. Cell Host Microbe *30*, 124-138.e8.
910 https://doi.org/10.1016/j.chom.2021.12.003.

79. Liu, C., Zhou, N., Du, M.-X., Sun, Y.-T., Wang, K., Wang, Y.-J., Li, D.-H., Yu, H.-Y., Song, Y., Bai, B.-B., et al. (2020). The Mouse Gut Microbial Biobank expands the coverage of cultured bacteria. Nat Commun *11*, 79. https://doi.org/10.1038/s41467-019-13836-5.

80. Giampazolias, E., Pereira da Costa, M., Lam, K.C., Lim, K.H.J., Cardoso, A., Piot, C., Chakravarty, P., Blasche, S., Patel, S., Biram, A., et al. (2024). Vitamin D regulates microbiome-dependent cancer immunity. Science *384*, 428–437. https://doi.org/10.1126/science.adh7954.

81. Pruss, K.M., Chen, H., Liu, Y., Van Treuren, W., Higginbottom, S.K., Jarman, J.B., Fischer, C.R., Mak, J., Wong, B., Cowan, T.M., et al. (2023). Host-microbe co-metabolism via MCAD generates circulating metabolites including hippuric acid. Nat Commun *14*, 512. https://doi.org/10.1038/s41467-023-36138-3.

82. Wilde, J., Slack, E., and Foster, K.R. (2024). Host control of the microbiome: Mechanisms, evolution, and disease. Science *385*, eadi3338. https://doi.org/10.1126/science.adi3338.

83. van Leeuwen, P.T., Brul, S., Zhang, J., and Wortel, M.T. (2023). Synthetic microbial communities (SynComs) of the human gut: design, assembly, and applications. FEMS Microbiol Rev *47*, fuad012. https://doi.org/10.1093/femsre/fuad012.

84. Raghu, A.K., Palanikumar, I., and Raman, K. (2024). Designing function-specific minimal microbiomes from large microbial communities. NPJ Syst Biol Appl *10*, 46. https://doi.org/10.1038/s41540-024-00373-1.

85. Quinn-Bohmann, N., Carr, A.V., Diener, C., and Gibbons, S.M. (2025). Moving from genome-scale to community-scale metabolic models for the human gut microbiome. Nat Microbiol *10*, 1055–1066. https://doi.org/10.1038/s41564-025-01972-2.

934 86. Langfelder, P., and Horvath, S. (2008). WGCNA: an R package for weighted correlation
935 network analysis. BMC Bioinformatics *9*, 559. https://doi.org/10.1186/1471-2105-9-
936 559.

937 87. Gu, Z. (2022). Complex heatmap visualization. Imeta *1*, e43.
938 https://doi.org/10.1002/imt2.43.

939 88. Schloss, P.D. (2023). The Riffomonas YouTube Channel: An Educational Resource To
940 Foster Reproducible Research Practices. Microbiol Resour Announc *12*, e0131022.
941 https://doi.org/10.1128/mra.01310-22.

942